Modelling the precipitation of NbC on dislocations in a-Fe

F. Perrard, Alexis Deschamps, Philippe Maugis

Modelling the precipitation of NbC on dislocations in α-Fe

F. Perrard [a,b], A. Deschamps [a,*], P. Maugis [b,1]

[a] *LTPCM, CNRS UMR 5614, Institut National Polytechnique de Grenoble, Domaine Universitaire, BP 75, 38 402 St. Martin d'Hères Cedex, France*
[b] *Arcelor Research, voie Romaine, BP 30320, 57283 Maizieres les Metz, France*

Abstract

A model has been developed for describing the precipitation of NbC on dislocations in ferrite in an Fe–C–Nb steel. This model is a continuous description of the classical laws for nucleation growth and coarsening, which are adapted to the specific case where precipitates only form on dislocations. This model is successfully applied on an extensive data set obtained by small-angle neutron scattering for a wide temperature range and two alloy contents. Using this model, it is possible to estimate the effects of process parameters on the final microstructure and, notably, it is shown that the initial dislocation density has a pronounced influence on the maximum precipitate density.

Keywords: Precipitation modelling; Heterogeneous precipitation; Niobium carbide; Steels; Dislocations

1. Introduction

There has been much activity in the last 10 years involving the modelling of precipitation kinetics of a solid solution in metallic alloys. A variety of modelling techniques are now available, which can efficiently describe an increasing level of complexity. Two main categories of models are available, which answer to separate purposes. The first describes precipitation in a great deal of detail, with very few assumptions, in an attempt to increase the understanding of nucleation. In this category, the kinetic Monte-Carlo [1–4] and the cluster dynamics techniques [5–7] are able to describe all stages of precipitation (from nucleation to coarsening) with a precise description of the kinetics involved in the system. However, many restrictions exist for the applicability of these models (e.g., high supersaturation, rigid lattice, CPU time, etc.) and therefore simpler models, based on the classical equations describing nucleation and growth, are widely used for most practically relevant situations [8]. Such simple models are again either found as ''class'' models, where the precipitate size distribution is discretised in classes, the evolution of which is calculated using a classical growth/dissolution law [9–11], or as ''integrated'' models, which integrate in time the differential equations of the classical nucleation, growth and coarsening laws in a continuous way [12,13]. Recent developments of this second category of models include the description of ternary systems [13], non-isothermal precipitation [11,14] and transition from metastable to stable phases [15].

One other type of complexity which can arise when modelling precipitation is heterogeneous precipitation on crystalline defects, notably on dislocations. The role of dislocations as favourable sites for precipitation has been thoroughly described by Larché some time ago [16]. Another prominent feature of the influence of dislocations on precipitation is short-circuit diffusion, leading to faster precipitation kinetics. On the macroscopic scale, this effect has often been simply introduced in classical precipitation models as a modified effective diffusivity [17–20]. Due to the change in the spatial distribution of the diffusion path,

* Corresponding author. Fax: +33 4 76 82 66 44.
E-mail address: alexis.deschamps@ltpcm.inpg.fr (A. Deschamps).
[1] Present address: CIRIMAT, CNRS, INP Toulouse, 118 route de Narbonne, 31077 Toulouse, France.

doi:10.1016/j.actamat.2006.10.003

Table 1
Chemical composition of high- and low-Nb alloys (weight ppm)

	Nb	C	N	S	P	Al	O
Low-Nb alloy	400	58	9	10	10	90	53
High-Nb alloy	790	110	10	23	10	60	13

the presence of dislocations leads to a change in the power of the coarsening law, first calculated by Kreye [21]. However, in the case where precipitation occurs only on dislocations, no model exists which would combine the current understanding of the effects of these defects on all three stages of precipitation.

In a previously published paper [22], a quantitative characterisation of the precipitation kinetics of NbC in α-iron has been carried out on two alloy compositions, in a wide range of temperatures (600–800 °C). Combining transmission electron microscopy (TEM) and small-angle neutron scattering (SANS), the following conclusions have been reached regarding precipitation in the range 600–800 °C:

- A specific feature of this system is a very high initial dislocation density. These dislocations result from the very fast austenite to ferrite transformation rate during quenching of the solution-treated austenitic phase. This dislocation density has been estimated by coupling TEM and SANS measurements to $2 \times 10^{14}\ \mathrm{m}^{-2}$.
- Precipitation of NbC occurs solely on dislocations; precipitates are moderately elongated (aspect ratio ~2–3) and regularly spaced on dislocations.
- Nucleation is always very fast; in fact, the number density of precipitates is observed to decrease from the first data point measured, even though the total volume fraction has hardly started to rise.
- A change in the power of the coarsening law (n where $r \propto t^n$) is observed, from ~1/5 to ~1/3 when the temperature is increased from 600 to 800 °C.
- Two alloys have been studied, with a factor of two in solute contents (see Table 1). The precipitation kinetics is almost insensitive to the solute content in this range.

This paper will present an adaptation of an "integrated" model [12] to the specific case of precipitation on dislocations, so that the specific experimental issues can be addressed. A previous publication [23] has shown that the classical models (which have been developed for homogeneous precipitation) are not capable of correctly describing the present experimental data set.

2. Description of the model

2.1. Overview

The present precipitation model is based on differential equations describing the instantaneous evolution of the average parameters of the microstructure, namely the average precipitate size and volume fraction (and the redundant parameters which are the precipitate density and matrix solute content). The precipitate size distribution is not directly taken into account: its influence on the coarsening stage, for instance, is implicitly present in the evolution law considered. The integration of the differential equations is carried out using an Euler algorithm.

The mechanism of precipitation on dislocations which has been identified in the experimental study will be described with as much detail as possible, in the following way:

(i) Precipitates are located only on dislocations; thus a specific nucleation law is necessary, with a reduced nucleation barrier as compared to homogeneous precipitation. The specific geometry of nucleation has also to be taken into account.
(ii) During growth and coarsening, dislocations act as diffusion short-circuits. Moreover, dislocations act as solute collectors; thus it is necessary to describe the diffusion of solute from the matrix to the dislocations and its redistribution on the precipitates located on the dislocations.

The following hypotheses will be used in this model:

- Precipitates are stoichiometric NbC, whose thermodynamics are given by a simple solubility product. The precipitation reaction is purely diffusion controlled, which means that the interface concentrations are given by a local equilibrium; in addition, the diffusion coefficient of niobium is very small as compared to that of carbon.
- There is no coupling between recovery and precipitation. We assume that if recovery of initially present dislocations occurs, it is finished when precipitation starts, so that dislocations can be safely assumed to be immobile during the precipitation process.
- For the sake of simplicity, precipitates are assumed to be spherical.

2.2. Nucleation and growth

Nucleation and growth are considered to occur simultaneously in this system, which means that new precipitates are allowed to nucleate while existing precipitates are in their growing stage. In this mixed nucleation and growth mode, the variation rate of the precipitate number density equals the nucleation rate J_n:

$$\left.\frac{\mathrm{d}N}{\mathrm{d}t}\right|_{n\&g} = J_n. \tag{1}$$

The growth rate of the average precipitate size depends on two components – the growth rate of existing precipitates of average size R and the arrival of new precipitates at the nucleation radius:

$$\left.\frac{dR}{dt}\right|_{n\&g} = \left.\frac{dR}{dt}\right|_{g} + \frac{1}{N} J_n (R^* - R), \tag{2}$$

where $\left.\frac{dR}{dt}\right|_g$ is the growth rate of existing precipitates and R^* is the critical radius at which the precipitates nucleate, which is defined as the size of the precipitates for which the interfacial equilibrium concentration is equal to the average solute concentration of the alloy (in Nb and C):

$$R^* = \frac{R_0}{\ln\left(X_{ss}^{Nb} X_{ss}^{C} / K^{\infty}\right)}, \tag{3}$$

where X_{ss}^{Nb} and X_{ss}^{C} are, respectively, the atom fractions of Nb and C in solid solution, K^{∞} is the solubility product of NbC precipitation in ferrite at a given temperature and R_0 is a capillarity radius defined as

$$R_0 = \frac{2\gamma V_{NbC}}{k_B T}, \tag{4}$$

where γ is the interfacial energy of the NbC precipitates and V_{NbC} is the molecular volume of NbC.

2.2.1. Nucleation rate

The stationary nucleation rate on dislocations J_S is simply derived from the homogeneous nucleation rate, taking a heterogeneous nucleation barrier ΔG^*_{Het} and a site nucleation density $\rho/\mathbf{b}$, where ρ is the dislocation density and $\mathbf{b}$ the Burgers vector:

$$J_s = Z\beta^* \frac{\rho}{b} \exp\left(-\frac{\Delta G^*_{Het}}{k_B T}\right), \tag{5}$$

where T is the temperature and k_B the Boltzmann constant. For the Zeldovich factor Z and the critical solute attachment rate β^*, we take the classical expressions:

$$Z = \frac{V_{NbC}}{2\pi R^{*2}} \sqrt{\frac{\gamma}{k_B T}}; \quad \beta^* = \frac{4\pi R^{*2} D_{Nb}^{Bulk} X_{ss}^{Nb}}{a^4}, \tag{6}$$

where D_{Nb}^{Bulk} is the bulk diffusion coefficient of niobium in ferrite and a is the ferrite lattice parameter. The heterogeneous nucleation barrier is simply considered to be proportional to the homogeneous one, α being an adjustable parameter of the model:

$$\Delta G^*_{Het} = \alpha \frac{16\pi\gamma^3}{3\Delta g^2} \quad \text{and} \quad \Delta g = -\frac{k_B T}{V_{NbC}} \ln\left(\frac{X_{ss}^{Nb} X_{ss}^{C}}{K^{\infty}}\right), \tag{7}$$

where Δg is the chemical driving force for nucleation. No transitory nucleation rate is considered here, since it has been calculated that the incubation time is very small compared to the overall nucleation period.

2.2.2. Criterion for the end of nucleation

In a situation where nucleation is homogeneous, nucleation stops as soon as the average solute content decreases due to the formation of precipitates. This induces a corresponding decrease of the driving force for nucleation in the remaining solid solution and the nucleation rate quickly comes to zero. The situation is quite different when heterogeneous precipitation occurs on dislocations. In this case, nucleation on dislocations is fed by solute diffusing from the bulk. An incoming solute atom arriving on a dislocation can either participate in the nucleation of a new precipitate, or diffuse rapidly along the dislocation to feed the growth of an existing precipitate (see Fig. 1a). If the second mechanism dominates, nucleation stops, even if the average solute content far from the dislocation has not significantly decreased from the initial value. A criterion for the end of the nucleation stage is described below. Note that the distance between two precipitates on a dislocation is on average $d = 1/N_{lin}$, where N_{lin} is the linear density of precipitates.

The average time δt_1 for nucleating a precipitate in between two existing precipitates can be estimated from the stationary nucleation rate J_s:

$$\delta t_1 = \frac{N_{lin}\rho}{J_s}. \tag{8}$$

On the other hand, the characteristic time for a solute on a dislocation to diffuse to an existing precipitate can be determined from the diffusion coefficient of the controlling species (niobium) along dislocations D_{Nb}^{disl}:

$$\delta t_2 = \frac{d^2}{2D_{Nb}^{disl}} = \frac{1}{2N_{lin}^2 D_{Nb}^{disl}}. \tag{9}$$

The probability of not forming a nucleus per unit time between two existing precipitates is thus written as:

$$p = \exp(-\delta t_2/\delta t_1) = \exp\left(-\frac{1}{2\rho N_{lin}^3 D_{Nb}^{disl}} J_s\right). \tag{10}$$

The actual nucleation rate on a dislocation is reduced by a factor $(1-p)$ that represents the proportion of Nb atoms on the dislocation that effectively contribute to nucleation. This yields the following expression of the real nucleation rate:

$$J_n = (1 - \exp(-\delta t_2/\delta t_1)) J_s. \tag{11}$$

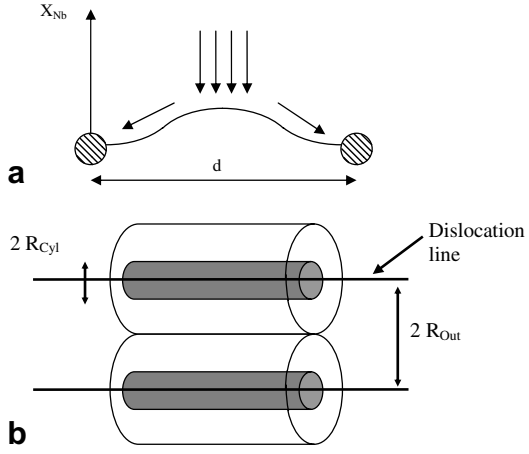

Fig. 1. Details of modelling. (a) Criterion for the end of nucleation. (b) Cylindrical geometry for diffusion with the two characteristics radii.

2.2.3. Growth

Owing to the very fast diffusion of Nb along dislocations compared to volume diffusion, we assume that during the growth regime the limiting process is the diffusion of niobium from the matrix towards the dislocations. In this case, the solute atoms arriving on the dislocations are assumed to be instantaneously redistributed on the precipitates present. We assume cylindrical diffusion geometry around each straight portion of a dislocation line (see Fig. 1b). Two boundary conditions have to be defined: one on the outer and one on the inner radius of a cylinder aligned on the dislocation line.

The outer radius is taken as the half-distance between two dislocations assumed to be parallel: $R_{\mathrm{Out}} = 1/2\sqrt{\rho}$. The corresponding solute concentration is the average solute content of the limiting species $X_{\mathrm{ss}}^{\mathrm{Nb}}$. The inner radius R_{Cyl} is the radius of a virtual cylindrical precipitate of the same volume per unit length of dislocation as that of the spherical precipitates:

$$R_{\mathrm{Cyl}} = \sqrt{\frac{4R^3 N_{\mathrm{lin}}}{3}}. \tag{12}$$

In the first stages of precipitation, R_{Cyl} may have a non-physically acceptable value. Thus, a minimum value of $2b$ is given to this parameter.

Given a solute flux J (in at. $\mathrm{m}^{-2}\,\mathrm{s}^{-1}$) coming to the inner radius, the mass balance on the cylindrical precipitate is

$$\frac{\mathrm{d}R_{\mathrm{Cyl}}}{\mathrm{d}t} = \frac{|J|}{\frac{1}{V_{\mathrm{NbC}}} - \frac{1}{V_{\mathrm{Fe}}} X_i^{\mathrm{Nb}}(R)}, \tag{13}$$

where V_{NbC} and V_{Fe} are the molecular volumes of NbC and ferrite, respectively.

Solving the diffusion equation in cylindrical co-ordinates gives the expression for the solute flux [24]:

$$|J| = \frac{D_{\mathrm{Nb}}^{\mathrm{Bulk}}}{R_{\mathrm{Cyl}} V_{\mathrm{Fe}}} \frac{X_{\mathrm{ss}}^{\mathrm{Nb}} - X_i^{\mathrm{Nb}}(R)}{\ln(R_{\mathrm{Out}}/R_{\mathrm{Cyl}})}, \tag{14}$$

where $X_i^{\mathrm{Nb}}(R)$ is the Nb concentration in the matrix in the vicinity of a spherical precipitate of radius R. This concentration is assumed to verify the local equilibrium at the interface, taking into account the Gibbs–Thomson effect in the form of a radius-dependent solubility product $K(R)$:

$$K(R) = X_i^{\mathrm{Nb}}(R) X_i^{\mathrm{C}}(R) = K^{\infty} \exp\left(\frac{R_0}{R}\right). \tag{15}$$

Eqs. (13) and (14) give the rate of growth of the virtual cylindrical precipitate:

$$\frac{\mathrm{d}R_{\mathrm{Cyl}}}{\mathrm{d}t} = \frac{D_{\mathrm{Nb}}^{\mathrm{Bulk}}}{R_{\mathrm{Cyl}}} \frac{X_{\mathrm{ss}}^{\mathrm{Nb}} - X_i^{\mathrm{Nb}}(R)}{V_{\mathrm{Fe}}/V_{\mathrm{NbC}} - X_i^{\mathrm{Nb}}(R)} \frac{1}{\ln(R_{\mathrm{Out}}/R_{\mathrm{Cyl}})}. \tag{16}$$

In this equation, the interfacial Nb concentration X_i^{Nb} is an unknown variable. Its expression can be derived from the flux compatibility constraint, as follows. Since precipitates remain stoichiometric, the solute fluxes of carbon and niobium towards the precipitate are equal and therefore:

$$D_{\mathrm{Nb}}^{\mathrm{Bulk}}\left(X_i^{\mathrm{Nb}}(R) - X_{\mathrm{ss}}^{\mathrm{Nb}}\right) = D_{\mathrm{C}}\left(X_i^{\mathrm{C}}(R) - X_{\mathrm{ss}}^{\mathrm{C}}\right). \tag{17}$$

Solving Eqs. (15) and (17) provides the interfacial concentration of Nb and C in equilibrium with precipitates of size R. It is worth noting that on account of the high diffusivity of carbon atoms relative to niobium atoms, the interfacial carbon concentration is almost equal to the average carbon content of the solid solution. On the other hand, the interfacial niobium concentration is mainly a function of this same average carbon content of the solid solution. This effect tends to an increase of X_i^{Nb} with time as the solid solution is progressively depleted in carbon. On the other hand, the Gibbs–Thomson effect tends to decrease the interfacial concentrations as the mean radius of the precipitates increases with time. The resulting time evolution of X_i^{Nb} towards its final equilibrium value is generally a non-monotonous one, even in isothermal conditions.

Finally, the growth rate of the "real" spherical precipitates is simply obtained by writing the volume conservation equation between cylindrical and spherical precipitates, which yields:

$$\left.\frac{\mathrm{d}R}{\mathrm{d}t}\right|_{\mathrm{g}} = \frac{2}{3}\left(\frac{3}{4R_{\mathrm{Cyl}}N_{\mathrm{lin}}}\right)^{1/3} \frac{\mathrm{d}R_{\mathrm{Cyl}}}{\mathrm{d}t}. \tag{18}$$

2.3. Growth and coarsening

2.3.1. Continuous description of the two stages

Growth and coarsening during an isothermal treatment can be described in a continuous way, As long as all precipitates are much larger than the critical radius, pure growth is valid: then the precipitate density is constant and the growth rate is given by Eq. (18). On the other hand, when the average radius reaches the critical radius, pure coarsening is valid: then the precipitate density decreases and a coarsening law for the growth rate of the average precipitate size has to be established. In between the two regimes, a transition can be considered [12]; we choose the following linear addition law for its simplicity:

$$\begin{aligned} \frac{\mathrm{d}R}{\mathrm{d}t} &= (1 - f_{\mathrm{coars}}) \left.\frac{\mathrm{d}R}{\mathrm{d}t}\right|_{\mathrm{g}} + f_{\mathrm{coars}} \left.\frac{\mathrm{d}R}{\mathrm{d}t}\right|_{\mathrm{Coars}}, \\ \frac{\mathrm{d}N}{\mathrm{d}t} &= f_{\mathrm{coars}} \left.\frac{\mathrm{d}N}{\mathrm{d}t}\right|_{\mathrm{Coars}}, \end{aligned} \tag{19}$$

where f_{coars} is the "fraction" of coarsening rate, which equals 0 in the pure growth regime and 1 in the pure coarsening regime. It is defined as a function of the ratio between the current volume fraction f_{v} and the equilibrium volume fraction, corrected by the Gibbs–Thomson effect, $f_{\mathrm{v}}^{\mathrm{eqGT}}$:

$$f_{\mathrm{coars}} = \mathrm{Sup}\left[1 - 100\left(\frac{f_{\mathrm{v}}}{f_{\mathrm{v}}^{\mathrm{eqGT}}} - 1\right)^2, 0\right]. \tag{20}$$

The equilibrium volume fraction corrected by the Gibbs–Thomson effect is the volume fraction obtained when the

matrix solute content is equal to the interfacial concentration of the precipitate of average size R. It is a function of the mean radius R, the temperature T and the nominal concentrations in the alloy X_0^{Nb} and X_0^{C}. From the matter balance of Nb atoms, f_v^{eqGT} can be written as:

$$f_V^{eqGT} = \left(X_0^{Nb} - X_{eq}^{Nb}(R)\right)(V_{NbC}/V_{Fe}), \tag{21}$$

where V_{NbC} and V_{Fe} are the volumes of one mole of, respectively, the NbC compound and the ferrite. The equilibrium concentration of Nb in solid solution, $X_{eq}^{Nb}(R)$, is calculated from:

$$X_0^{Nb} - X_{eq}^{Nb}(R) = X_0^{C} - X_{eq}^{C}(R) \tag{22}$$

and

$$X_{eq}^{Nb}(R)X_{eq}^{C}(R) = K(R), \tag{23}$$

where Eq. (22) is a mass balance and Eq. (23) is the local equilibrium condition at the precipitate/matrix interface.

The specific form of the function f_{coars} in Eq. (20) has been designed to insure that the mixing Eq. (19) be valid beyond the simple case of an isothermal treatment for precipitate growth: indeed, they have been numerically checked to be valid for isothermal and non-isothermal heat treatments in cases of growth ($f_v < f_v^{eq}$), as well as in cases of dissolution ($f_v > f_v^{eq}$) of the precipitates. Its evolution is shown in Fig. 2.

2.3.2. Coarsening rate

During coarsening, solute exchange between the precipitates can occur either by volume diffusion, or by pipe diffusion along the dislocations. When solute exchange occurs only by volume diffusion, the growth rate is simply given by the well known LSW equation, which in our case expresses [25,26]:

$$\left.\frac{dR}{dt}\right|_{Bulk} = \frac{4}{27}\frac{X_{ss}^{Nb}\cdot R_0\cdot D_{Nb}^{Bulk}}{V_{Fe}/V_{NbC} - X_{ss}^{Nb}}\left(\frac{1}{R^2}\right). \tag{24}$$

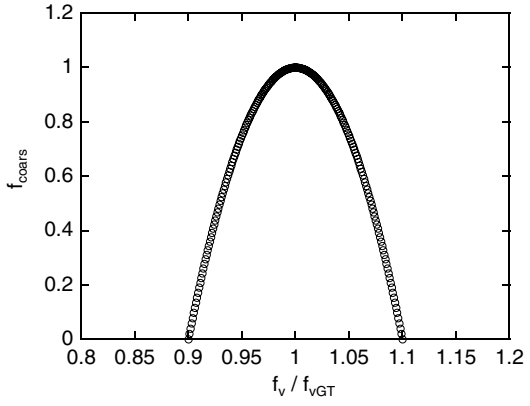

Fig. 2. Value of the fraction of coarsening versus the ratio between the volume fraction and the maximum volume fraction including Gibbs–Thomson correction. When f_v/f_v^{GT} is <0.9 or >1.1, f_{coars} is kept equal to 0.

When solute exchange occurs only by pipe diffusion along dislocations, and when one precipitate is connected only to one dislocation, the growth rate has been solved by Kreye [21]:

$$\left.\frac{dR}{dt}\right|_{Disl} = 2\times 10^{-2} X_{ss}^{Nb} R_0 D_{Nb}^{disl} R_{Pipe}^2\left(\frac{1}{R^4}\right), \tag{25}$$

where R_{Pipe} is the radius around the dislocation below which the pipe diffusion coefficient can be used. We will consider that $R_{Pipe} = 2b$.

When both mechanisms operate simultaneously, one has to make an approximation to obtain an analytical expression for the growth rate. Following Iwashita and Wei [27], we will consider that these two growth rates can be evaluated in parallel and simply added:

$$\left.\frac{dR}{dt}\right|_{Coars} = \left.\frac{dR}{dt}\right|_{Bulk} + \left.\frac{dR}{dt}\right|_{Disl}. \tag{26}$$

From this equation, it results that when the precipitates are very small, the relative surface area of pipe diffusion (πR_{Pipe}^2) is large and thus the growth rate is dominated by pipe diffusion; when the precipitates are very large, the solute exchange area is dominated by the matrix and the growth rate equals the LSW expression. The transition between the two regimes occurs around a critical radius R_{trans}, which depends on the ratio between the volume and dislocation diffusion coefficients:

$$R_{trans} = \sqrt{\frac{D_{Nb}^{disl}}{D_{Nb}^{Bulk}}b^2}. \tag{27}$$

For instance, if the diffusivity ratio is 10^3, the transition will be observed for a radius of ~20 nm. If this ratio is 10^5, the transition radius will be 200 nm.

From Eq. (26), the growth rate of the average precipitate size is known. In the coarsening regime, according to the LSW theory, the average radius equals the critical radius at all times. Thus:

$$R^*(t) = R(t) \tag{28}$$

and

$$f_v(t) = f_v^{eqGT}(t), \tag{29}$$

where $f_v(t)$ is the precipitated volume fraction and $f_v^{eqGT}(t)$ is the equilibrium volume fraction for precipitates of size R^*. The number density of precipitates at time $t + dt$ can thus be calculated:

$$N_{coars}(t+dt) = \frac{f_v(t+dt)}{\frac{4}{3}\pi\left(R(t) + \left.\frac{dR}{dt}\right|_{Coars}dt\right)^3} \tag{30}$$

and

$$\left.\frac{dN}{dt}\right|_{Coars} = \frac{(N_{coars}(t+dt) - N_{coars}(t))}{dt}. \tag{31}$$

2.4. Transition from nucleation to coarsening

The transition between the nucleation and growth to the growth and coarsening regimes is simply considered when the precipitate number density decrease by coarsening is larger than the nucleation rate:

$$-\left.\frac{dN}{dt}\right|_{Coars} > J_n. \quad (32)$$

We checked that in all modelled conditions both fluxes in precipitate number density had negligible values at the time of the transition, so that the details of the transition had no influence on the overall model predictions.

3. Model calibration and comparison with experimental results

3.1. Parameters

Literature data concerning NbC precipitation are quite limited, namely interfacial energy, solubility product and diffusion coefficients. In order to limit the number of adjustable parameters, we have used two kinds of parameters: those which can be taken from the literature with an acceptable accuracy and those that are adjustable.

Concerning literature parameters, we have used the solubility product of NbC in ferrite proposed by Turkdogan [28] and the Nb diffusion coefficient in ferrite based on Refs. [29,30]. We will allow a slight adjustment from this literature value. The dislocation density has been experimentally determined as 2×10^{14} m^{-2} [22].

Thus, the only adjustable parameters of the model are:

- the ratio $D_{Nb}^{disl}/D_{Nb}^{Bulk}$, which should lie between 10^3 and 10^7 to be physically acceptable; we will assume that it is constant with temperature in the studied range;
- the interfacial energy γ, which can safely be assumed to lie in the interval 0.3–1 J m^{-2}; we will assume that it is constant with temperature in the studied range;
- the nucleation parameter α, which is comprised in the range 0–1.

The model is then calibrated on the experimental data for the high-Nb alloy used in the experimental study presented in [22] (Table 1), aged at 600, 700 and 800 °C. Model parameters are given in Table 2 and the comparison between the experimental data and model predictions is given in Fig. 3.

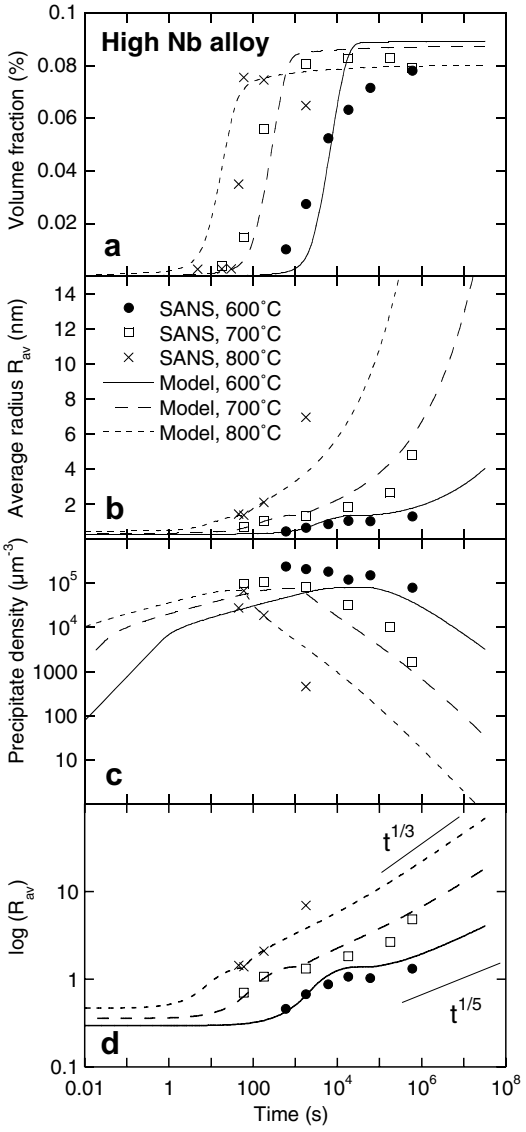

Fig. 3. Comparison between experimental and modelling results for three isothermal heat treatments (high-Nb alloy).

Before detailing the model predictions, a few comments can be made on the value of the model parameters:

- the nucleation parameter α is very low; this means that the nucleation barrier on dislocations is very much reduced as compared to homogeneous nucleation; this point will be further discussed below;
- the solubility product is taken directly from Turkdogan [28]; however, the diffusion constant is slightly adjusted from the literature data;

Table 2
Set of parameters used to adjust the model on experimental data

K (wt.%)		D_{Nb}^{Bulk}		D_{Nb}^{disl}				
A	B	D_0 (m^2 s^{-1})	Q (kJ mol^{-1})	D_0 (m^2 s^{-1})	Q (kJ mol^{-1})	α	γ (J m^{-2})	ρ (m^{-2})
9830	4.33	1.27×10^{-5}	224	1.27×10^{-2}	224	0.01	0.5	2×10^{14}

- the ratio between the dislocation and volume diffusion constants is lower than expected from the literature ($\sim 10^5$); however, the value of 1000 is sufficient to validate the hypotheses of the model (criterion for the end of nucleation and cylindrical diffusion morphology).

3.2. Description of the experimental data

Figs. 3 and 5 show the comparison between the model output and the experimental results, in terms of radius, volume fraction and precipitate density, on the high- and low-Nb materials, respectively (see Table 1 for alloy compositions), with the same set of parameters.

For both alloys, and for the three temperatures, results are well described by the model. More precisely, at 700 and 800 °C, the model prediction corresponds particularly well to the results, in all three stages of precipitation. However, the solubility product that was used imperfectly describes the equilibrium volume fraction at the lowest solubility studied, namely the low-Nb alloy at 800 °C.

At 600 °C, the model predictions are a little less convincing. The nucleation rate predicted by the model is insufficient (especially for the high-Nb alloy), leading to an underestimation of the maximum precipitate density. Moreover, the overall extent of the kinetics (which can be defined as the time difference between 10% and 90% transformed) is significantly smaller than that measured experimentally. It should be stressed that this situation is much less pronounced as compared to homogeneous precipitation models [23]. A possible explanation is that precipitates are likely to be coherent in the first stages, which would slow down their growth rate, until they progressively lose coherency, thus widening the time-scale of the total precipitation process. However, we do not have clear experimental data to support this hypothesis.

The evolution of the mean radius in logarithmic scale is shown in Fig. 3d. This representation enables the comparison of the coarsening kinetics for the different temperatures. At 800 °C, the model prediction at long times shows a 1/3 exponent. At 600 °C, the model seems to evolve towards a 1/5 exponent, which stems from the lower precipitate size and Eq. (26). At 700 °C the exponent lies in between. Although we do not have experimental results at ageing times sufficiently long fully to validate these model predictions, the available data are compatible with this exponent change.

A more thorough look into the coarsening exponent is shown in Fig. 4, where the time exponent n ($R \propto t^n$) is continuously shown as a function of time for the three temperatures. At 800 °C, it can be seen that the exponent gradually becomes equal to 1/3: this means that pipe diffusion has become negligible in the coarsening kinetics. At 700 °C, the exponent is intermediate between 1/5 and 1/3 continuously in the investigated range. At 600 °C, coarsening starts very late (between 10^6 and 10^7 s) and never establishes at a 1/5 exponent: although the kinetics is dominated by pipe-diffusion ($n \sim 0.2$), the exponent continuously increases due to the increase in precipitate size.

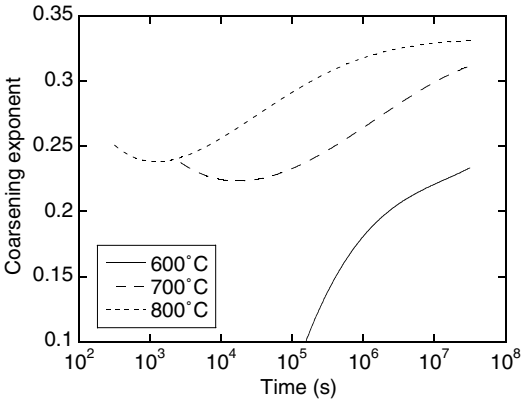

Fig. 4. Evolution of the time exponent $n = \frac{d \log R_{sw}}{d \log t}$ during the late stage of ageing for the high-Nb alloy at three temperatures: 600, 700 and 800 °C.

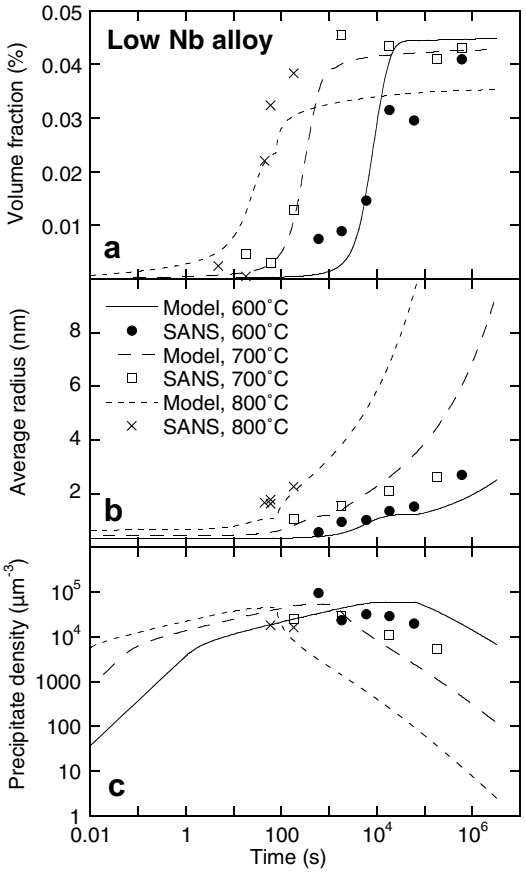

Fig. 5. Comparison between experimental and modelling results for three isothermal heat treatments (low-Nb alloy).

3.3. Predicted evolution of the microstructural parameters during ageing

Fig. 6 shows the detail of the various microstructural parameters for a specific case of ageing (namely high-Nb alloy, 700 °C). The evolution of volume fraction is shown

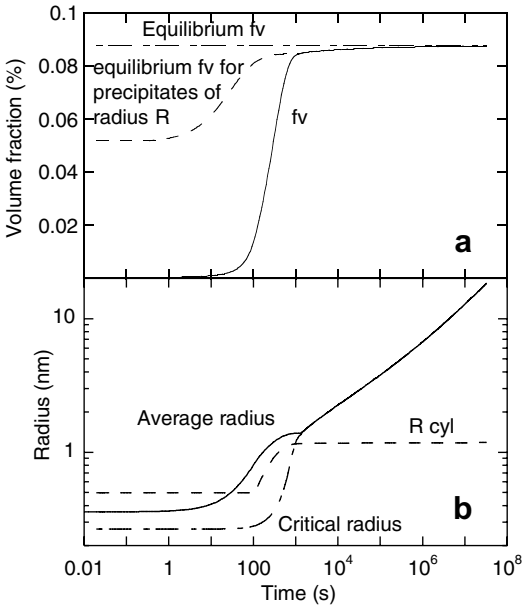

Fig. 6. Evolution of various model parameters during aging at 700 °C (high-Nb alloy).

concurrently with the evolution of the Gibbs–Thomson-corrected equilibrium volume fraction (i.e., the maximum volume fraction which can be reached with precipitates of size R). This comparison shows the importance of the Gibbs–Thomson correction for evaluating the driving force for growth in the first stages following nucleation; as expected, these two parameters converge at the onset of coarsening. The various relevant size parameters are also shown together; the critical radius is equal to the average radius in both the nucleation and coarsening stages; only in the growth stage are they very different, corresponding to the stability of most particles present in the precipitate size distribution. The characteristic size that we have called the "radius of equivalent cylindrical precipitate" is also represented. It is almost constant during coarsening, since it represents the total amount of solute precipitated per unit length of dislocation, which is almost constant during this stage. It is also constant in the early stages of precipitation, due to the fact that we impose a minimum value of $2b$ so that the solution of the diffusion field around the dislocation retains a physical meaning. Finally, the evolution of the precipitate density reflects a very short stage of pure growth, illustrating the necessity of treating all stages of precipitation concurrently.

3.4. Parametric study

The model can now be used to predict the influence of some important parameters; this can serve in either the study of the effect of changing some process parameters on the final steel microstructure, or in the estimation of the sensitivity of the model to some physical parameter.

We can, for instance, study the influence of the density of dislocations, since they serve as sole nucleation sites. Moreover, it can be expected that this parameter is sensitive to the exact quenching path of the material during the austenite to ferrite transformation. Fig. 7 shows the predicted evolution of the volume fraction and size and density of precipitates as a function of the dislocation density. In first approximation, the maximum number of precipitates is directly proportional to the density of nucleation sites; this results from our criterion which states that the end of nucleation is controlled locally at the level of the inter-particle distance and not by the average solute content. This has important consequences, notably on the growth stage: when the density of dislocations is very high, nucleation ends only when a significant amount of solute has been consumed. Therefore, the growth stage is almost absent and one goes continuously from nucleation to coarsening. In contrast, when the dislocation density is low, the model predicts a long stage of growth, leading to very coarse precipitate sizes. It should be stressed that it is extremely difficult to have access to low dislocation densities in such materials. In order to obtain a "clean" ferrite, the austenite to ferrite transformation needs to be slowed down, which inevitably induces the high-temperature precipitation of coarse NbC. Conversely, it is not certain that a higher initial dislocation density would lead to higher density of precipitates, since recovery is known to be very

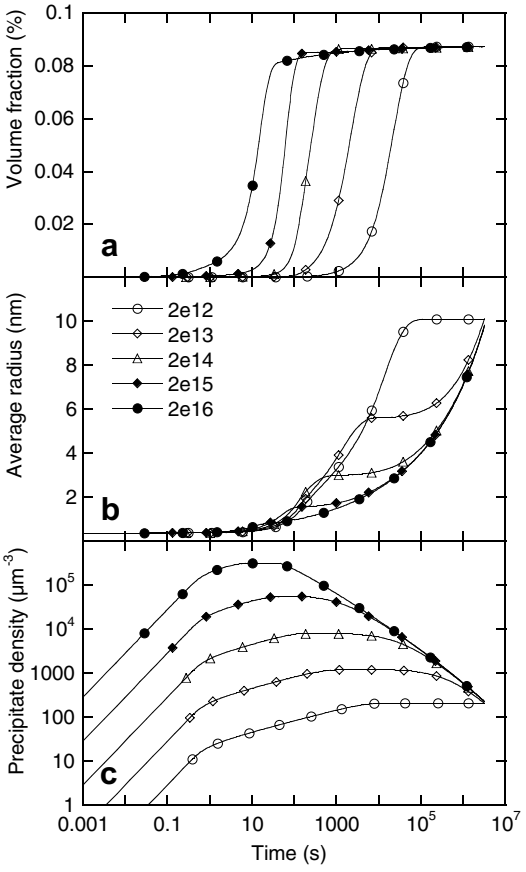

Fig. 7. Parametric study for the high-Nb alloy at 700 °C. All parameters are kept constant from those in Table 2 except for $\alpha = 0.4$, and on the dislocation density which is varied between 2×10^{12} and 2×10^{16} m^{-2}.

fast in ferrite and may happen before the nucleation stage in the temperature range investigated. As an indirect proof of this, we have actually observed that a pre-deformation of the samples has little effect on the precipitation kinetics [31].

It is also worth evaluating the influence of the ratio between the volume and dislocation diffusivities of niobium, which is very poorly known and had to be adjusted in the experiments. Fig. 8 shows that this parameter is actually of paramount importance to the precipitation characteristics. It actually has virtually no effect on the precipitated volume fraction (which is mainly controlled by the volume diffusion of solute towards the dislocations), but directly controls the maximum density of precipitates, through the criterion for the end of nucleation. Moreover, it has a direct influence on the kinetics of coarsening, via the respective weights of the volume- or dislocation -controlled mechanisms (see Eqs. (22) and (23)).

3.5. Comparison with other data in the literature

One other study in the literature by Gendt et al. [32] provides quantitative data on the precipitation kinetics in the Fe–Nb–C system, with a slightly different composition (6.3×10^{-4} at.% Nb and 4.2×10^{-4} at.% C). The volume fraction of precipitates has in this case been determined by thermo-electric power and the precipitate size by TEM. As shown in Fig. 9, our model, with the set of parameters given in Table 2, matches relatively well this set of data, even though it underestimates the precipitate sizes at higher temperatures. However, it must be pointed out that precipitate sizes were measured on carbon replicas; in these conditions the smallest precipitates can be missed.

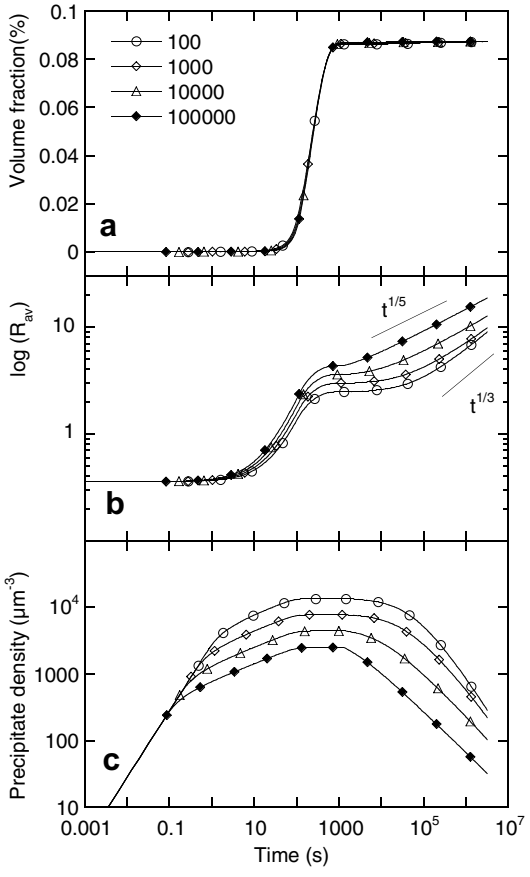

Fig. 8. Parametric study for the high-Nb alloy, at 700 °C. All parameters are kept constant with those in Table 2 except for $\alpha = 0.4$ and the diffusion coefficient of Nb along dislocations, which is adjusted so that $D^{disl}_{Nb}/D^{Bulk}_{Nb}$ varies between 10^2 and 10^5.

3.6. Discussion of the model hypotheses

We have shown in the present modelling approach that the activation barrier for nucleation on dislocations has to be greatly lowered compared to bulk nucleation (by a factor of 100) so that the experimental results can be reproduced. A number of effects can participate in this decrease, as discussed below.

(i) Relief by the dislocation of the elastic misfit between precipitate and matrix. In fact, if they are coherent, the NbC precipitates have a strong misfit in all directions with the iron matrix [33] (10% along the ⟨1 1 0⟩ directions of NbC parallel to the ⟨1 0 0⟩ directions of ferrite and 50% in the ⟨1 0 0⟩ directions of NbC parallel to the ⟨1 0 0⟩ directions of ferrite). However, a detailed study of the nature of dislocations on which NbC precipitates form shows that the Burgers vector does not fully participate in the relief of this misfit strain [34].

(ii) The molar volume of NbC is twice that of ferrite. Thus, when a niobium solute incorporates a precipitate, the accompanying vacancy may be trapped

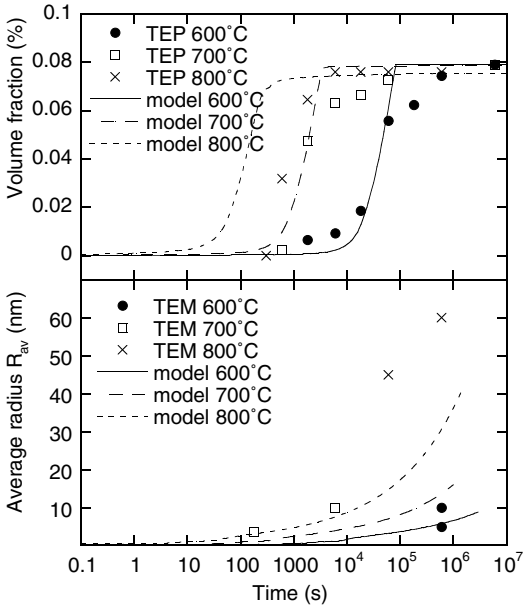

Fig. 9. Comparison between experiments and modelling results for the data obtained by Gendt et al. [32].

simultaneously. For diffusion to go on, vacancy sources have to be activated in the material. Dislocations can be such sources, which would favour precipitation in their vicinity. However, a dislocation, covered with precipitates, cannot climb very much from its original position in order to provide vacancies. We can take as an example the high-Nb alloy, aged for 3000 min at 700 °C, for which we know the precipitate size and density. It is then possible to calculate that the entire dislocation length would have to have climbed 9 nm high in order to provide enough vacancies for all the precipitates present in the sample. Nothing of this kind has been seen by TEM observations. Thus we conclude that if a vacancy-assisted growth mechanism is at work, the dislocations are not likely to be the controlling source of these vacancies.

(iii) Solute segregation, either of carbon or niobium, can be of great importance. If segregation occurs before nucleation, it can significantly increase the solute content at the dislocation (although the net effect can also be to stabilise the free solute at the expense of the precipitate stability). If segregation occurs after nucleation, it can be an additional driving force for solute diffusion towards the dislocation and thus increase the precipitate growth rate.

In first approximation, we will assume that the segregation energies of carbon and niobium at the dislocations are the same as on grain boundaries, and that segregated carbon and niobium do not interact. The segregation energies have been determined for carbon as $\Delta G_c = 80$ kJ mol^{-1} [35] and for niobium as $\Delta G_{Nb} = 38$ kJ mol^{-1} [36]. From these energies, it is possible to calculate the equilibrium concentrations of the two species at the dislocations (X_C^D and X_{Nb}^D), as a function of the matrix concentrations (X_C^M and X_{Nb}^M) and temperature [37,38]:

$$X_C^D = \frac{1}{1 + X_C^M \exp(-\Delta G_C/RT)} \quad \text{and}$$
$$X_{Nb}^D = \frac{1}{1 + X_{Nb}^M \exp(-\Delta G_{Nb}/RT)}. \tag{33}$$

For the high-Nb alloy, the equilibrium concentrations are shown in Table 3. The segregation of carbon is very strong, which should result in the immediate presence of a higher carbon content at the dislocations. In the case of niobium, the effect is less pronounced, but can still accelerate the diffusion of solute towards the dislocation. In order to assess the magnitude of this effect compared to that of "normal" diffusion, we can compare the solute fluxes resulting on the one hand from the concentration gradient and on the other hand from the elastic interaction with the dislocation.

Table 3
Segregation ratio of Nb and C for the high-Nb alloy at two temperatures

	600 °C	800 °C
X_C^D/X_C^M	1.9×10^3	1.6×10^3
X_{Nb}^D/X_{Nb}^M	172	67

The solute flux resulting from the concentration gradient is that already used for the present model. It can be written as:

$$|J| = \left(\frac{1}{V_{NbC} - \frac{1}{V_{Fe}} X_i^{Nb}}\right) \left.\frac{dR}{dt}\right|_{Cyl}. \tag{34}$$

The solute flux resulting from the elastic strain field of the dislocation can be evaluated by the Cottrell–Bilby model, which applies to solute segregation on edge dislocations. At short segregation times, the number of moles of solute segregating per unit length of dislocation can be written as [39]:

$$N(t) = 3C_o \left(\frac{\pi}{2}\right)^{1/3} \left(L D_{Nb}^{Bulk}\right)^{2/3} t^{2/3}, \tag{35}$$

where C_o is the solute concentration and L is a parameter which depends on the size difference between the solute and matrix atoms [39,40]:

$$L = \frac{A}{kT} \quad \text{where} \quad A = \frac{4}{3}\mu\varepsilon r_{Fe}^3 b \left(\frac{1+\nu}{1-\nu}\right), \tag{36}$$

where $\mu = 83$ GPa is the shear modulus of iron, $\nu = 0.3$ is Poisson's ratio, $r_{Fe} = 0.126$ nm is the atomic radius of iron and $r_{Fe}(1+\varepsilon)$ that of niobium ($\varepsilon = 0.15873$).

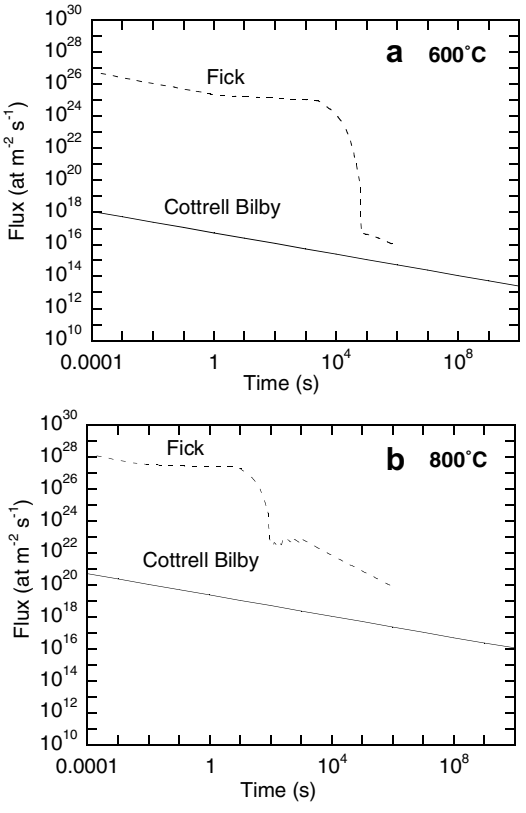

Fig. 10. Comparison between the fluxes driven by the concentration gradient (Fick) and by elastic interaction (Cottrell–Bilby) for two temperatures.

The contribution of segregation can finally be written as a flux of atoms by unit area and time:

$$J_{\text{segr}} = \frac{X_{\text{Nb}}}{V_{\text{Fe}}} \frac{1}{\pi R_{\text{Cyl}}} \left(\frac{\pi}{2}\right)^{1/3} \left(LD_{\text{Nb}}^{\text{Bulk}}\right)^{2/3} t^{-1/3}. \quad (37)$$

Of course, this segregation flux is only valid in the case when one is far from solute saturation at the dislocations. This is likely to be the case here, since the solute arriving at the dislocation is then trapped on the precipitates.

The comparison of the two fluxes (driven by the concentration gradient and driven by the elastic interaction) is shown in Fig. 10 for two temperatures, namely 600 and 800 °C. In both cases, the flux due to the concentration gradient is largely dominant, which validates our modelling hypotheses. It is interesting to note that tomographic atom probe observations by Bémont [41] on early stages of ageing have actually shown carbon segregation at the dislocations, but no niobium segregation.

4. Conclusions

A continuous model, based on the classical theory for nucleation, growth and coarsening, has been developed specifically for the case where precipitation only occurs on dislocations.

The features of this model which are specific to precipitation on dislocations are the following:

- a modified nucleation law and a modified criterion for the end of nucleation, taking into account the competition between nucleation of new precipitates and growth of existing ones;
- a growth law, controlled by the volume diffusion of solute to the dislocations, which is calculated for a cylindrical geometry;
- a coarsening law, taking into account the exchange of solute both through the matrix and along the dislocation lines.

Using this model, an extensive experimental data set (providing the precipitate size and density) has been successfully described, on a wide range of temperatures and for two solute contents, with a very limited number of parameters. Notably, the specific features of this data set have been correctly described, namely:

- in the range of our study, the solute content of the alloy has little effect on the precipitation kinetics; his stems naturally from our criterion for the end of nucleation stage;
- the change in the coarsening kinetics from $t^{1/5}$ at low temperature to $t^{1/3}$ at high temperature arises from the higher precipitate sizes encountered in the latter case.

This model enables the prediction of the effects of changing some process parameters on the final microstructure and, notably, the dislocation density, which has a strong influence on the maximum precipitate density.

Acknowledgements

This work was part of a French scientific program (CPR Précipitation), in collaboration with Arcelor, Pechiney, CNRS, CEA, INPG, INSA Lyon, Université de Rouen, Université Aix-Marseille III and LEM-ONERA. Professor Y. Bréchet, Dr. M. Goune and Dr. C. Scott are thanked for fruitful discussions.

Appendix A. Supplementary material

Supplementary data associated with this article can be found, in the online version, at doi:10.1016/j.actamat.2006.10.003.

References

[1] Clouet E, Nastar M, Sigli C. Nucleation of Al3Zr and Al3Sc in aluminum alloys: from kinetic Monte Carlo simulations to classical theory. Phys Rev B 2004;69:064109/1.

[2] Fratzl P, Penrose O. Kinetics of spinodal decomposition in the Ising model with vacancy diffusion. Phys Rev B 1994;50:3477.

[3] Soisson F, Barbu A, Martin G. Monte Carlo simulations of copper precipitation in dilute iron–copper alloys during thermal aging and under electron irradiation. Acta Mater 1996;44:3789.

[4] Soisson F. Applications of Monte Carlo simulations to the kinetics of phase transformations. NATO Sci Ser II: Math Phys Chem 2003;108:427.

[5] Kampmann R, Ebel T, Haese M, Wagner R. A combined cluster-dynamic and deterministic description of decomposition kinetics in binary alloys with a tendency for clustering. Phys Status Solidi B 1992;172:295.

[6] Hardouin Duparc A, Moingeon C, Smetniansky-de-Grande N, Barbu A. Microstructure modelling of ferritic alloys under high flux 1 MeV electron irradiations. J Nucl Mater 2002;302:143.

[7] Christien F, Barbu A. Modeling of copper precipitation in iron during thermal aging and irradiation. J Nucl Mater 2004;324:90.

[8] Wagner R, Kampmann R. Homogeneous second phase precipitation. Materials science and technology: a comprehensive treatment, vol. 5. Weinheim: Wiley–VCH; 1991. p. 213.

[9] Myhr OR, Grong O. Modelling of non-isothermal transformations in alloys containing a particle distribution. Acta Mater 2000;48:1605.

[10] Robson JD. A new model for prediction of dispersoid precipitation in aluminium alloys containing zirconium and scandium. Acta Mater 2004;52:1409.

[11] Nicolas M, Deschamps A. Characterisation and modelling of precipitate evolution in an Al–Zn–Mg alloy during non-isothermal heat treatments. Acta Mater 2003;51:6077.

[12] Deschamps A, Brechet Y. Influence of pre-deformation and ageing of an Al–Zn–Mg alloy. II. Modeling of precipitation kinetics and yield stress. Acta Mater 1998;47:293.

[13] Buessler P, Maugis P, Bouaziz O, Schmitt J-H. Integrated process-metallurgy modeling: example of precipitation during coil cooling. Iron Steelmaker 2003;30:33.

[14] Deschamps A, Genevois C, Nicolas M, Perrard F, Bley F. Study of precipitation kinetics: towards non-isothermal and coupled phenomena. Philos Mag 2005;85:3091.

[15] Perez M, Deschamps A. Microscopic modelling of simultaneous two-phase precipitation: application to carbide precipitation in low-carbon steels. Mater Sci Eng A 2003;360:214.

[16] Larché FC. Nucleation and precipitation on dislocations. In: Nabarro FRN, editor. Dislocations in solids, vol. 4. Amsterdam: North Holland; 1979.

[17] Hart EW. Acta Mater 1957;5:597.
[18] Frost HJ, Ashby MF. Deformation-mechanism maps. Oxford: Pergamon Press; 1982.
[19] Dutta B, Palmiere EJ, Sellars CM. Modelling the kinetics of strain induced precipitation in Nb microalloyed steels. Acta Mater 2001;49:785.
[20] Zurob HS, Hutchinson CR, Bréchet Y, Purdy GR. Modelling recrystallization of microalloyed austenite: effect of coupling recovery, precipitation and recrystallization. Acta Mater 2002;50:3075.
[21] Kreye H. Z Metallkd 1970;61:108.
[22] Perrard F, Deschamps A, Bley F, Donnadieu P, Maugis P. A small-angle neutron scattering study of fine-scale NbC precipitation kinetics in the α-Fe–Nb–C system. J Appl Crystallogr 2006;39:473.
[23] Perrard F, Deschamps A, Maugis P, Donnadicu P, Bley F. Characterization and modeling of NbC precipitation in model microalloyed steels. In: Solid state transformation and heat treatment [European congress and exhibition on advanced materials and processes held at Euromat 2003], 8th, Lausanne, Switzerland, September 1–5, 2003; 2005. p. 3.
[24] Adda Y, Philibert J. La diffusion dans les solides: Bibliothèques des sciences et techniques nucléaires; 1966.
[25] Lifshitz IM, Slyozov VV. The kinetics of precipitation from supersaturated solid solutions. J Phys Chem Solids 1961;19:35.
[26] Wagner C. Z Elektrochem 1961;65:581.
[27] Iwashita CH, Wei RP. Coarsening of grain boundary carbides in a nickel-based ternary alloy during creep. Acta Mater 2000;48:3145.
[28] Turkdogan ET. Iron Steelmaker 1968:61.
[29] Geise J, Herzig C. Lattice and grain boundary diffusion of niobium in iron. Z Metallkd 1985;76:622.
[30] Herzig C, Geise J, Divinski SV. Niobium bulk and grain boundary diffusion in alpha-iron. Z Metallkd 2002;93:1180.
[31] Perrard F, Deschamps A, Donnadieu P, Maugis P. Characterization and modeling on NbC heterogeneous precipitation in model IF steels. In: Material science and technology 2004, New Orleans, LA, United States, September 26–29, 2004, vol. 1; 2004. p. 31.
[32] Gendt D, Maugis P, Bouaziz O, Lanteri S, Barges P. Modelling of niobium carbide precipitation in steel. In: COM: Conference of Metallurgists. Ottawa: Canadian Institute of Mining, Metallurgy and Petroleum, Montreal, Canada; 2000. p. 16.
[33] DeArdo AJ, Gray JM, Meyer L. Fundamental metallurgy of niobium in steel. In: Stuart H, editor. International symposium niobium. San Francisco, CA: TMS-AIME; 1984. p. 685.
[34] Perrard F, Donnadieu P, Deschamps A, Barges P. TEM study of NbC heterogeneous precipitation in ferrite. Philos Mag 2006;86:4271.
[35] Misra RD, Weatherly GC, Embury D. Kinetics of cold work embrittlement in rephosphorised, interstitial free steels. Mater Sci Technol 2000;16:9.
[36] Maruyama N, Smith GDW, Cerezo A. Interaction of the solute niobium or molybdenum with grain boundaries in alpha-iron. Mater Sci Eng A 2003;353:126.
[37] McLean D. Grain boundaries in metals. London: Clarendon Press; 1957.
[38] Guttmann M. Grain boundary segregation and embrittlement in multicomponent systems: recent literature revisited. In: The Donald McLean symposium: structural materials engineering application through scientific insight. Teddington, National Physical Laboratory, The Institute of Materials; 1995.
[39] Bullough R, Newman RC. The kinetics of migration of points defects to dislocations. Rep Prog Phys 1970;33:101.
[40] Bullough R, Newman RC. The flow of impurities to an edge dislocation. Proc R Soc A 1962;249:427.
[41] Bémont E. Précipitation de carbures et de carbonitrures dans la ferrite. vol. PhD. Rouen: Université de Rouen, France; 2003.